RC beams strengthened in shear using the Embedded Through-Section technique: experimental results and analytical formulation

Authors: Breveglieri M. [1], Aprile A.[2], Barros J.A.O.[3]

[1] PhD student, ENDIF, Dep. of Eng., University of Ferrara, 44121 Ferrara, Italy, matteo.breveglieri@unife.it

[2] Assistant Professor, ENDIF, Dep. of Eng., University of Ferrara, 44121 Ferrara, Italy, alessandra.aprile@unife.it

[3] Full Professor, ISISE, Dep. of Civil Eng., Univ. of Minho, Azurém, 4810-058 Guimarães, Portugal, barros@civil.uminho.pt

Abstract

The Embedded Through-Section (ETS) is a recent strengthening technique that has been developed to retrofit existing reinforced concrete (RC) elements with shear reinforcement deficiencies. This technique is based on the execution of holes drilled through the element cross section, in which steel or fiber reinforced polymer (FRP) bars are inserted and bonded to the surrounding concrete with an epoxy adhesive. An experimental program was carried out with RC T-cross section beams strengthened in shear using steel ETS bars. The influence of the inclination and shear strengthening ratio of ETS on the shear strengthening efficiency was evaluated, as well as the interaction of ETS bars with existing steel stirrups. Two different analytical models are presented in this paper in order to calculate the contribution of ETS to shear resistance. The first model follows an empirical approach (experimental-based approach), while the second model takes into account the physical and mechanical principles of the technique (mechanical-based approach). The predictive performance of both models is assessed by using the experimental results.

Keywords: Embedded Through-Section technique, B. Debonding, C. Analytical modelling, D. Mechanical testing.

1. Introduction

The Embedded Through-Section (ETS) is an effective technique for the shear strengthening of reinforced concrete (RC) elements. This technique is based on the execution of holes drilled through the element cross section, in which steel or fiber reinforced polymer (FRP) bars are inserted and bonded to the surrounding concrete with an epoxy adhesive. Different FRP-

based strengthening techniques, like Externally Bonded Reinforcement (EBR) and Near Surfaces Mounted (NSM), are being investigated and applied for the shear strengthening of RC beams; however the ETS technique was proved to be particularly efficient, providing a significant increase of shear resistance, usually higher than the one attained by using NSM and EBR techniques [1–5]. The ETS technique is also a cost competitive and feasible solution when EBR and NSM techniques cannot be applied [6].

Like any FRP-based strengthening technique, the ETS technique relies its efficiency on the bond between the concrete substrate and the strengthening element; furthermore, the bond effectiveness is influenced by the provided confinement [7–9]. In fact, unlike the case of EBR simply glued on the concrete surface, a certain confinement obtained in the NSM FRP strips due to the insertion into thin slits open in the concrete cover allows to develop high bond stress. Oehlers et al. [10] demonstrated experimentally that by installing NSM strips into deeper grooves the bond performance can be improved. An even higher confinement, which entails advantages on the bond strength, is obtained for ETS installed bars due to the deep embedment into the concrete core of the element to be strengthened. Perrone et. al. [11] improved the bond performance of CFRP-NSM strips embedded in the concrete cover of RC columns by increasing the confinement effect through a hybrid strengthening solution.

To apprise the performance of the ETS technique for the shear strengthening of RC beams, an experimental program was carried out by using steel ETS bars. Three series of beams with different percentage of existing steel stirrups were tested with the purpose of evaluating the influence of the internal shear reinforcing ratio, as well as the influence of the percentage and inclination of the ETS bars on the strengthening effectiveness. A detailed description of the experimental program and the discussion of the results are presented in Breveglieri et al. [4,5].

The high number of parameters affecting the shear behavior makes this phenomenon quite complex and not yet completely addressed. The parameters that influence the shear behavior of a strengthened RC element were already identified [12–14]. International guidelines on the use of FRPs [15–18] take into account only a restricted number of factors, ignoring the influence, for instance, of existing transverse reinforcement.

Considering the experimental results obtained by the authors and previous experimental works [1,3], two different analytical formulations are assessed and presented herein in order to predict the contribution of the steel ETS bars for the shear strengthening of RC beams. The first approach, named *experimental-based*, is supported by the concept of effective strain, like the most of the existing approaches. The calculation of the effective strain can be performed using empirical equations [19–22] or using a bond model [23]. The second approach, named *mechanical-based*, is derived by modifying the simplified formulation proposed by Bianco et al. [24], originally developed for CFRP strips

applied according to the NSM technique. This latest is a comprehensive three-dimensional model developed fulfilling equilibrium, kinematic compatibility and constitutive laws of the materials involved, as well as the local bond between the involved materials. [7,25,26].

2. Experimental Program

2.1 Test series

The experimental program is composed by fifteen T cross section beams divided in three Series (Series 0S, 2S, 4S). Fig.1 presents the geometry and the reinforcement details of the tested series. The reinforcement system was designed, using a high percentage of longitudinal reinforcement (ρ_{sl} =2.79%), in order to force the occurrence of shear failure mode for all the beams of the experimental program. To localize shear failure in one of the beam's shear spans, a three point load configuration was selected, with a different length of the beam's shear spans. The monitored beam's span (L_1 =0.9 m) is 2.5 times the effective depth of the beam's cross section (L_1/d =2.5). As shown in Fig.2, different shear reinforcement systems were applied in the L_1 beam's span of the tested beams: 0S-Series does not have conventional steel stirrups, 2S-Series has steel stirrups ϕ 6@300 mm, corresponding to a shear reinforcement ratio ρ_{sw} = 0.10%, and 4S-Series has steel stirrups ϕ 6@180 mm, corresponding to a shear reinforcement ratio ρ_{sw} = 0.17%. Table 1 indicates the designation adopted for each beam and the strengthening configurations, namely, the number of applied ETS bars, inclination, spacing, shear strengthening ratio (ρ_{fw}), as well as the percentage of steel stirrups (ρ_{sw}) and total shear reinforcement ($\rho_{sw} + \rho_{fw}$). Each series has a reference beam without ETS strengthening system, and four beams with different ETS strengthening configurations (Fig. 2). The investigated parameters were the shear strengthening ratio (ρ_{fw}) and the inclination (90°, 45°) of the ETS bars, as well as the influence of the percentage of existing steel stirrups. The diameter of the ETS steel bars was 10 mm. The ETS strengthening ratio varied between 0.15% (ETS bars at 90° spaced at 300 mm) and 0.34% (ETS bars at 45° and spaced at 180 mm). As an example, in Fig. 2 are represented the four strengthening configurations (beams 0S-S300-90, 2S-S300-45, 2S-S180-90 and 4S-S180-45). The concrete average compressive strength (f_{cm}) of the beams at the age of the beams' test (approximately 250 days) was equal to 29.7 for 0S-Series and 2S-Series, and 32.3 MPa for 4S-Series. The adopted 10 mm diameter ETS bars were of the same steel class of the bars used for the flexural reinforcement and steel stirrups of the beams (f_y =549 MPa, ε_{sy} = 0.275% and Young's modulus of 200 GPa) and they were bonded to the concrete substrate using the Sikadur 32 N epoxy based adhesive. More details can be found in Breveglieri el al. [4,5].

2.2Analysis of the experimental results

2.2.1 Behavior of a RC beam shear strengthening with ETS bars

The typical load (F)-deflection (u_L) diagram for the 2S-Series is presented Fig.3. All the tested beams showed the same behavior up to the formation of the first diagonal crack, that formed at an approximate load of 113 kN (u_L =0.98mm), 100 kN (u_L =0.91mm) and 135 kN (u_L =1.37mm) in case of the reference beams 0S-Ref, 2S-Ref and 4S-Ref, respectively. The ETS steel bars offered resistance to crack opening and sliding by bridging the shear cracks and enhancing concrete's contribution to the shear resistance due to the aggregate interlock effect. The ETS strengthened beams showed a higher load carrying capacity after shear crack initiation, and higher stiffness retention in comparison to the unstrengthened beams [27]. All of the beams exhibited shear failure mode, since a quite high flexural reinforcement ratio was adopted in order to avoid flexural failure mode. Fig. 4 shows the failure crack patterns for selected tested beams. The main results of the experimental tests are presented in Table 2, where $F_{\max}$ is the maximum load attained by the beams and $u_{L\max}$ is the displacement in the loaded section at $F_{\max}$. The strengthening efficiency of the ETS technique can be evaluated by considering the ratio $\Delta F/F_{\max,\mathrm{Re}f}$, where $F_{\max,\mathrm{Re}f}$ is the maximum load of the reference beam, and $\Delta F = F_{\max} - F_{\max,\mathrm{Re}f}$ is the increase of maximum load provided by each ETS arrangement. The Table 2 also includes the maximum shear force V_t =0.6 $F_{\max}$ applied in the L_1 beam's span (Fig. 1) and the resisting shear force provided by the ETS arrangement, $V_f^{\exp}$. Finally Table 2 includes the average inclination of the critical diagonal crack (CDC), determined by connecting the points of the interception of the critical shear crack with the bottom surface of the beam's flange and the longitudinal reinforcement, as represented in Fig. 4 for 0S-S300-90 beam. By considering all the tested beams, an average value of the inclination angle of the CDC equal to 44° was obtained. This angle exhibited the tendency to increase with the shear reinforcement ratio, as already observed in previous studies on FRP shear strengthened structures [28,29]. From the crack patterns presented in Fig. 4 it can also be observed that the number of diagonal cracks increases with the percentage of total shear reinforcement. The 0S-Series is characterized by the absence of stirrups in the strengthened shear span (ρ_{sw} = 0.0%); the beams of this series presented the highest strengthening efficiency amongst the tested series, with an increase of load carrying capacity that ranged from 40% to 136%. For the ETS vertical bars, the beams with the lowest percentage of ETS bars, ρ_{fw} = 0.15%

(0S-S300-90), and with the highest percentage, ρ_{fw} = 0.24% (0S-S180-90), presented an increase of load carrying capacity of 39.5% ($F_{\max}$ = 217.8 kN; $u_{L\max}$ = 4.37 mm) and 64.6% ($F_{\max}$ = 256.8 kN; $u_{L\max}$ =4.31 mm), respectively. The highest increase of load carrying capacity was obtained with ETS bars inclined at 45°. In fact the beams with the lowest percentage, ρ_{fw} = 0.24% (0S-S300-45) and with the highest percentage, ρ_{fw} = 0.34% (0S-S180-45) presented an increase of load carrying capacity of 123.4% ($F_{\max}$ =348.6 kN) and of 136.3% ($F_{\max}$ = 368.8 kN; $u_{L\max}$ =6.56 mm), respectively.

The 2S-Series (Fig.3) is shear reinforced with 2-arms ϕ 6 mm steel stirrups @300 mm (ρ_{sw} = 0.10%). For the ETS vertical bars, the beams with the lowest percentage of ETS bars, ρ_{fw} = 0.15% (2S-S300-90), and with the highest percentage, ρ_{fw} = 0.24% (2S-S180-90), presented an increase of load carrying capacity of 30.4% ($F_{\max}$ = 315.7 kN; $u_{L\max}$ =5.32 mm) and 68.1% ($F_{\max}$ = 406.8 kN; $u_{L\max}$ = 8.27 mm), respectively. Like already occurred in the beams of the 0S-Series, in the 2S-series the highest strengthening effectiveness occurred in the beams with ETS bars inclined at 45°. In fact, the beam with the lowest percentage of ETS bars, ρ_{fw} = 0.24% (0S-S300-45), and with the highest percentage, ρ_{fw} = 0.34% (2S-S180-45), presented an increase of the load beam carrying capacity of 68.2% ($F_{\max}$ =407.1 kN; $u_{L\max}$ =7.03 mm) and 108.5% ($F_{\max}$ = 504.7 kN; $u_{L\max}$ = 8.37 mm), respectively.

The 4S-series is shear reinforced with 2-arms ϕ 6 mm steel stirrups @180 mm (ρ_{sw} = 0.17%). For the ETS vertical bars, the beams with the lowest percentage of ETS bars, ρ_{fw} = 0.15% (4S-S300-90), and with the highest percentage, ρ_{fw} =0.24% (4S-S180-90), presented an increase of load carrying capacity of 4.8% ($F_{\max}$ = 370.9 kN; $u_{L\max}$ = 7.43mm) and 16.8% ($F_{\max}$ = 413.2 kN; $u_{L\max}$ = 6.32mm), respectively. The decrease of the shear strengthening effectiveness with the increase of existing shear reinforcement was quite evident. Furthermore, for the configuration 4S-S300-90, a $V_f^{\exp}$ = 10.3 kN was obtained, which is a quite small strengthening contribution. This evidence is justified by the fact that the shear failure crack was only crossed by one ETS bar, which developed a very small resisting bond length (Fig. 4). The results of this beam showed the importance of the adopted strengthening geometry, revealing that strengthened elements should be placed in between stirrups [3,30]. These results clearly evidence that an analytical model for estimating the contribution of ETS bars must consider the eventual occurrence of a bond failure mode, expecially in case of vertical installed bars. For the beams with ETS bars inclined at 45° a higher increase of load carrying capacity was obtained. In fact, the beams with the lowest percentage of ETS bars, ρ_{fw} = 0.24% (4S-S300-45), and with the highest percentage, ρ_{fw} =0.34% (4S-S180-45),

presented an increase of load carrying capacity of 56.1% ($F_{\max}$ =552.4 kN; $u_{L\max}$ = 12.03 mm) and 60.1% ($F_{\max}$ = 566.4kN; $u_{L\max}$ =11.01mm), respectively.

The recorded strain values [4,5] are dependent on the available bond length of the elements on which they are installed. In the vertical ETS bars the yield strain was usually attained in the elements that crossed the CDC at half of the beam's height (Beam 0S-S180-90, Fig. 4) since in this case the available bond length was adequate. If this available bond length is relatively small, the ETS bars cannot attain the yield strain due to slip occurrence. This implies that the contribution to shear resistance of a single ETS bar depends on its available bond length, as already demonstrated for EBR and NSM techniques [19,28,31–33]. Higher strains, that exceed the yield strain, have been in general recorded in inclined ETS bars, since this strengthening configuration assures larger bond transfer length. In some of the tested beams strengthened with inclined bars, the excellent bond conditions provided by the concrete core allowed the steel yield strain to be exceeded in more than one section of the same ETS bar crossing shear cracks. By using inclined bars, strain values higher than 0.8% were recorded in at least one of the ETS steel bars. Steel stirrups showed a trend in terms of strain variation similar to the ETS bars, attaining relatively high strains in the sections crossed by a diagonal crack. Moreover, the excellent anchorage conditions provided by the closed stirrups, as well as its smaller diameter (when compared to the ETS steel bars diameter), have assured the attainment of the yield strain in several sections monitored with strain gauges. In some of the beams, the steel stirrups have even attained its rupture (2S-S300-45, 4S-S180-90).

2.2.2. ETS steel bars failure mode

The ETS shear strengthening system mainly failed due to the debonding at the bar/adhesive interface. Due to the higher confinement provided to the ETS bars by the web-flange surrounding concrete under compression, debonding occurred in the bond length of ETS bars localized in the bottom part of the beam's cross section (apart 0S-S300-90, see Fig. 4), and generally in the shorter embedded length of the two parts in which the crack divided the ETS bar. During the opening and sliding process of this type of cracks, the vertical and inclined ETS bars that cross these cracks were submitted to axial and transversal force components leading the ETS bars to scratch the surrounding epoxy adhesive. This type of failure was also reported by Valerio et al. [1], and Dalfré et al. [34]. Despite this observed behavior, the bond performance was capable to mobilize the yield stress of the steel bars, even in the beams strengthened with the highest percentage of ETS bars. Previous research on EBR and NSM techniques revealed that a crack pattern with smaller crack spacing can accelerate the FRP debonding and lead to a premature failure, since the bond length is decreased by the formation of several cracks [28,35].

ETS strengthening is generally characterized by crack spacing larger than EBR and NSM techniques, therefore, the resulting ETS crack pattern does not seems to influence significantly the bond performance. The types of failures reported by Bianco et al. [36], namely, concrete fracture and mixed concrete-fracture-debonding did not occur in the present experimental program, due to the relatively high confinement provided by the concrete core surrounding the ETS bars. However, it is not possible to exclude the occurrence of this type of failures in case of using lower concrete strength class, or higher bars diameter, since in this latter case the generated tensile force that has to be equilibrated by the surrounding concrete is higher [34]. The tendency to the detachment of the concrete cover with the increase of the shear strengthening percentage, observed when using the NSM technique [27,37,38], was not observed in the ETS technique. Due to the scratching of the epoxy adhesive, the relatively small bond transfer length, and the absence of anchorage mechanisms, the maximum strain recorded in the ETS bars never attained the steel ultimate strain, and therefore the rupture of the steel ETS bars did never occur.

2.2.3. Influence of the percentage of existing steel stirrups on the ETS strengthening

As already demonstrated in beams strengthened with the ETS [2,3], EBR and NSM techniques [38–41], the effectiveness of the ETS strengthening system decreases with the increase of the shear reinforcement ratio of existing steel stirrups, ρ_{sw}. In Fig. 5 the influence of ρ_{fw} on the contribution of the ETS strengthening system, $V_f^{\exp}$ is represented. It was verified that for a given value of ρ_{fw}, the ETS strengthening effectiveness increased with the decrease of ρ_{sw}, being this tendency attenuated when inclined ETS bars were used. The higher shear effectiveness showed by the ETS inclined bars can be justified by considering that the orientation of the diagonal cracks tends to be almost orthogonal to the ETS bars, providing larger bond length than the case of the ETS vertical bars. As demonstrated by Bianco et al. [26,36], in case of shear strengthening elements with non-closed geometric configurations, such is the case of EBR and NSM reinforcements, the effective bond length has paramount influence on the shear strengthening effectiveness, since a bond length less than the critical one limits the strengthening effectiveness of the system. Fig. 5 also shows that the ETS shear strengthening effectiveness increased with the value of ρ_{fw}.

3. Analytical formulations

3.1 Strategy for the development of the analytical formulation

Two models are proposed for the prediction of the contribution of ETS bars for the shear strengthening of RC beams. For the assessment of the predictive performance of these models, the strengthening contribution of the ETS bars, V_f^{ana}, is determined by applying the following (Eq.1):

$$V_f^{ana} = V_t - V_{Ref} \tag{1}$$

Where V_{Ref} is the shear resistance of the reference beam, and V_t is the shear resistance of the ETS strengthened beam. Following this approach, it is assumed that the steel stirrups offer the same contribution in the strengthened and in the corresponding reference beams.

One model, herein designated as *experimental-based approach* (Section 3.2), is based on the evaluation of the effective strain ε_{fe}, which is estimated through an empirical approach that takes into account the total stiffness of the shear reinforcement and strengthening $\left(E_{fw}\rho_{fw} + E_{sw}\rho_{sw}\right)$ and the average concrete compressive strength, f_{cm}. Similar approaches have been used to evaluate the shear resistance of NSM and EBR systems [19–22], and have also been adopted by international codes [15,16].

The other model, herein designated as *mechanical-based model* (Section3.3), follows the modelling strategy described by Bianco et al. [24]. This latter is a simplified version of a more sophisticated three-dimensional mechanical model developed to predict the NSM-FRP shear strengthening contribution for RC beams, considering different physical phenomena, such as debonding and progressive concrete fracture process [7,25,36,42]. The *mechanical-based model* is based on the evaluation of an equivalent average bond length that takes into account the concrete fracture as a reduction effect of the average resisting bond length. This model also adopts a simplified bilinear rigid-softening bond-slip diagram. This formulation, presented in section 3.3, will be modified herein in order to be applicable for the ETS technique.

Both approaches have been developed adopting the variable angle truss model [43]. As reported by Bianco et al. [24], the CDC inclination is a function of the shear span-depth ratio (L_1/d) [44,45], of the shear reinforcement ratio ρ_{sw}, and of the percentage of shear strengthening ratio ρ_{fw}. As shown in Table 2, the average inclination of the CDC of the tested beams was 44°. Therefore, the currently used value of 45° for the critical diagonal crack inclination, θ, is adopted for both approaches.

3.2 Experimental-based model

The experimental-based model estimates the contribution of the ETS strengthening system for the shear resistance of a RC element by determining the effective strain in the ETS bars ε_{fe}, which corresponds to the average strain in steel when the strengthened RC beam reaches its shear capacity. This empirical approach follows the procedure proposed for the NSM technique by Dias and Barros [22]. The force resulting from the tensile stress in the ETS bars crossing the shear failure crack, F_f, is given by the following Eq. (2):

$$F_f = n_f \cdot A_{fw} \cdot f_{fe} \tag{2}$$

where f_{fe} is the effective stress in the ETS bar, which is obtained multiplying the Young's modulus of the bars, E_{fw} by the effective strain, ε_{fe}. This force is limited by the yield force. In Eq. (2) A_{fw} is the cross sectional area of the shear reinforcement, and is given by Eq. (3):

$$A_{fw} = n\frac{\pi \cdot \phi_f^2}{4} \tag{3}$$

where ϕ_f is the ETS bar diameter and n is the number of bars installed in the considered cross section. Finally n_f is the number of ETS bars crossed by the shear failure crack, given by Eq. (4):

$$n_f = \frac{h_w \cdot \left(\cot\beta_f + \cot\theta\right)}{s_{fw}} \tag{4}$$

where h_w (Fig. 6) is the depth of the cross section, θ is the orientation of the shear failure crack (CDC), β_f is the inclination of the ETS bar with respect to the beam's axis, and s_{fw} is the spacing of ETS bars.

The vertical projection of the force, F_f, is the contribution of the ETS bars for the shear resistance of the beam, V_f^I:

$$V_f^I = F_f \cdot \sin\beta = n_f \cdot A_{fw} \cdot f_{fe} \cdot \sin\beta_f \tag{5}$$

Introducing Eq. (4) into Eq. (5) and considering the constitutive law for the ETS bars ($f_{fe} = E_{fw} \cdot \varepsilon_{fe}$) it results:

$$V_f^I = h_w \cdot \frac{A_{fv}}{s_{fw}} \cdot \varepsilon_{fe} \cdot E_{fw} \cdot \left(\cot\theta + \cot\beta_f\right) \cdot \sin\beta_f \tag{6}$$

By considering for V_f^I the values obtained experimentally, ($V_f^I = V_f^{\exp}$) the previous equation can be used for determining the effective strain:

$$\varepsilon_{fe} = V_f^{\exp} \Bigg/ \left(h_w \cdot \frac{A_{fv}}{s_{fw}} \cdot E_{fw} \cdot \left(\cot\theta + \cot\beta_f\right) \cdot \sin\beta_f \right) \tag{7}$$

The concept of effective strain to evaluate the shear contribution of the strengthening is usually applied to FRP strengthened elements [19–22], in which the strengthening material exhibits a linear elastic behavior up to failure. Since steel bars are used in the present work, the assumption of a linear elastic behavior can be used exclusively to calculate an effective strain ε_{fe}. In the case of steel ETS bars, the strengthening material exhibit an elastic-plastic behavior and the effective stress, $f_{fe} = E_{fw} \cdot \varepsilon_{fe}$, is limited by the yield stress f_y. In section 4.1 the effective strain (ε_{fe}^{I}) to be used for the evaluation of the shear strengthening contribution of the ETS system, V_f^I, will be obtained by best fitting the experimental ε_{fe} recorded values.

3.3 Mechanical-physical based model

The mechanical-based approach herein proposed follows the main simplifications proposed by Bianco et al. [24] to their original model [26]. The CDC can be schematized as an inclined plane dividing the beam in two parts, joined together by the ETS bars crossing the plane. For the presented approach it is assumed that the inclined critical diagonal crack (CDC) at each load step assumes a constant opening along its entire length [46], unlike what adopted by [42,47]. At each load step the two parts moves apart and the opening of the crack, i.e. distance between these parts, increases. The ETS bars oppose to the crack opening by anchoring to the surrounding concrete and transferring the bond force originated by the imposed slip δ_{Li}. The capacity of an ETS bar depends on its available bond length L_{fi} that is the shorter between the two parts into which the crack divides its actual length L_f (Fig 7a). The local bond stress-slip curve is represented by a simplified bi-linear curve (Fig.7b), in which it is possible to identify the “rigid”, “softening friction”, “free-slipping” phases [24,42]. The rigid branch $\left(0-\tau_0\right)$ represents the initial shear strength, for which the value τ_0 expresses and average strength of the physical properties of the steel-adhesive-concrete interface. For an imposed slip, it is assumed that the stresses are transferred by friction and micromechanical interlock. These shear reinforcement mechanisms decrease with the increase of the slip (softening friction) up to the point $\delta_{Li} = \delta_1$ in which the friction resisting mechanism is exhausted, leading to a free-slipping phase with the evolution of the crack opening. The constitutive bond law $V_{fi}^{bd}\left(L_{Rfi}, \delta_{Li}\right)$ is determined by simulating the behavior of a simple ETS bar within a concrete prism (Fig. 7c and d), whose dimensions are limited by the spacing between adjacent bars and half of the web cross section width, $b_w/2$. This assumption is adopted in order to

neglect the interaction between ETS bars in the beam's axis direction, otherwise the formulation of the model becomes too complex for an engineer-design framework. If more than one ETS bars are installed in the cross section, it is possible to have an interaction effect in the orthogonal direction to the beams' axis, and the value $b_w/2$ should be reduced taking into account the geometry of the cross section. However, this is expected to be a non-current situation for the majority of RC beams requiring shear strengthening intervention. The interaction with existing stirrups is neglected, due to the complexity of the phenomenon, a topic that requires dedicated research. The steel embedded bar-concrete cone system can exhibit the failure modes represented in Fig. 7d: debonding, bar yielding, concrete conical fracture and mixed shallow conical-plus-debonding. The fracture occurs when the stress in the concrete surrounding the bar attains the tensile strength. The shape of this surface can be conventionally assumed as a cone with the principal generatrices inclined of an angle α with respect to the bar longitudinal axis [7,42]. The cracking propagation increases with the imposed slip, and the resisting bond length decreases progressively. In this simplified approach the concrete fracture process is accounted by reducing the bar resisting bond length L_{Rfi} by using the factor η ($0 \le \eta \le 1$), which is a function of the average tensile strength f_{ctm}^{*}. This last is calculated imposing the equality between the maximum force that can be transferred through bond stress, and the force corresponding to the concrete conical fracture. For values of $f_{ctm} \ge f_{ctm}^{*}$ concrete does not fracture, and $\eta = 1$. The effective capacity $V_{fi,eff}^{\max}$ of a single ETS bar is obtained adopting the minimum value between the yield strength and the bond strength and using the equivalent value of the average bond length, $\overline{L}_{Rfi}^{eq} = \eta L_{Rfi}$ [24].

3.3.1 Proposed design formula

The input parameters include the following geometrical and mechanical data: the beam cross-section web's height h_w and width b_w, inclination angle of both CDC and ETS bars with respect to the beam's longitudinal axis, θ and β_f, respectively, bars spacing measured along the beam's axis, s_{fw}, diameter ϕ_f of the ETS bar, concrete average compressive strength f_{cm}, steel yield strength f_y and Young's modulus E_{fw}. Other parameters strictly related to the proposed model are: the angle α ETS bar's axis and principal generatrices of the conical fracture surface (Fig. 7c-d), bond stress τ_0 and slip δ_1 defining the adopted local bond stress-slip relationship (Fig.7b). The algorithm of this model is described in Fig.8, which will be detailed in the following sections.

3.3.2 Average value of the available resisting bond length $\bar{L}_{Rfi}$ and minimum number of bars $N^l_{f,\text{int}}$ effectively crossing the CDC

The average value of the available bond length ($\bar{L}_{Rfi}$), and the minimum integer number of bars effectively crossing the CDC ($N^l_{f,\text{int}}$) are determined according to the recommendations of Bianco et al. [36]. The $N^l_{f,\text{int}}$ is obtained by rounding off the real number to the lowest integer as follows:

$$N^l_{f,\text{int}} = \text{round off}\left[h_w \cdot \frac{\left(\cot\theta + \cot\beta_f\right)}{s_{fw}} \right] \tag{8}$$

while $\bar{L}_{Rfi}$ is determined from:

$$\bar{L}_{Rfi} = \frac{1}{N^l_{f,\text{int}}} \cdot \sum_{i=1}^{N^l_{f,\text{int}}} L_{fi} \tag{9}$$

where (Fig. 7a):

$$L_{fi} = \begin{cases} i \cdot s_{fw} \cdot \dfrac{\sin\theta}{\sin(\theta+\beta_f)} & for \quad x_{fi} < \dfrac{h_w}{2} \cdot \left(\cot\theta + \cot\beta_f\right) \\ L_f - i \cdot s_{fw} \cdot \dfrac{\sin\theta}{\sin(\theta+\beta_f)} & for \quad x_{fi} \geq \dfrac{h_w}{2} \cdot \left(\cot\theta + \cot\beta_f\right) \end{cases} \tag{10}$$

and:

$$x_{fi} = i \cdot s_{fw} \tag{11}$$

If $s_f \geq h_w$ the calculation of the average bond length gives a null length (Eq. (9)); in these cases $\bar{L}_{Rfi} = \left(h_w \cdot \sin\theta \cdot \left(\cot\theta + \cot\beta_f\right)\right) \Big/ \left(4 \cdot \left(\sin\theta + \sin\beta_f\right)\right)$ is adopted [24].

3.3.3 Evaluation of Constants

The geometrical and integration constants characterizing the bond transfer mechanism are obtained from Eq. (12) to Eq. (19).

The perimeter of the bar cross section:

$$L_p = \phi_f \pi \tag{12}$$

The cross section area of the relevant prism of surrounding concrete:

$$A_c = s_f \cdot \frac{b_w}{2} \tag{13}$$

$$L_d = \frac{h_w}{\sin\theta} \tag{14}$$

The ETS bar yield force:

$$V_f^y = \frac{\pi \cdot \phi_f{}^2}{4} f_y \tag{15}$$

Concrete mean tensile strength:

$$f_{ctm} = 1.4 \cdot ((f_{cm} - 8)/10)^{\frac{2}{3}} \tag{16}$$

Concrete's Young's modulus:

$$E_c = 2.15 \cdot 10000 \cdot (f_{cm}/10)^{\frac{1}{3}} \tag{17}$$

where both E_c and f_{ctm} are herein evaluated by means of the CEB-FIP Model Code 1990 formulation [48], with f_{ctm} in MPa.

The bond-modeling constants are obtained from the following Eqs. (18) and (19).

Integration constants regarding the bond transfer mechanism J_1 and $1/\lambda^2$:

$$J_1 = \frac{L_p}{A_{fw}} \cdot \left[\frac{1}{E_{fw}} + \frac{A_f}{A_c \cdot E_c} \right]; \quad \frac{1}{\lambda^2} = \frac{\delta_1}{\tau_0 \cdot J_1}; \tag{18}$$

The effective resisting bond length L_{Rfe} , and the corresponding maximum bond force V_{f1}^{bd} :

$$L_{Rfe} = \frac{\pi}{2 \cdot \lambda}; \; V_{f1}^{bd} = \frac{L_p \cdot \lambda \cdot \delta_1}{J_1} \tag{19}$$

More details on the evaluation of these model's constants are reported in Appendix A.

3.3.4 Reduction factor η and equivalent value of the average resisting bond length $\bar{L}_{Rfi}^{eq}$

The reduction factor can be evaluated as follows:

$$\eta\left(s_f; b_w; f_{cm}; \bar{L}_{Rfi}\right) = \begin{cases} \left(f_{ctm} / f_{ctm}^*\right)^{0.5} & if \quad f_{ctm} < f_{ctm}^* \\ 1 & if \quad f_{ctm} \geq f_{ctm}^* \end{cases} \tag{20}$$

where, (see Appendix A):

$$f_{ctm}^{*}=\frac{L_p\cdot\lambda\cdot\delta_1\cdot\sin\left(\lambda\cdot L_{Rfi}\right)}{J_1\cdot\pi\cdot\min\left\{L_{Rfi}\cdot\tan\alpha;\frac{b_w}{4}\right\}\cdot\frac{\sin\left(\theta+\beta_f\right)}{2}\cdot\left(\min\left\{\frac{s_{fw}\cdot\sin\beta_f}{2\cdot\sin\left(\theta+\beta_f\right)};\frac{L_{Rfi}\cdot\sin\alpha}{\sin\left(\beta_f+\theta+\alpha\right)}\right\}+\min\left\{\frac{s_{fw}\cdot\sin\beta_f}{2\cdot\sin\left(\theta+\beta_f\right)};\frac{L_{Rfi}\cdot\sin\alpha}{\sin\left(\beta_f+\theta-\alpha\right)}\right\}\right)} \tag{21}$$

in which L_{Rfi} has to be set equal to:

$$L_{Rfi}=\begin{cases}\bar{L}_{Rfi} & if \quad \bar{L}_{Rfi}\le L_{Rfe}\\ L_{Rfe} & if \quad \bar{L}_{Rfi}> L_{Rfe}\end{cases} \tag{22}$$

The function that defines the reduced embedded length, η, has relevant influence on the results of the model. In the present approach, η is assumed to be a square root function of f_{ctm}/f_{ctm}^{*} when $f_{ctm}<f_{ctm}^{*}$ (Eq. (20)), while a linear function was adopted by Bianco et al. [24]. This option provides higher value for $\bar{L}_{Rfi}^{eq}$, which is in agreement with the experimental results, where a visible concrete cone failure was never observed. The equivalent value of the average resisting bond length is given by Eq. (23):

$$\bar{L}_{Rfi}^{eq}=L_{Rfi}\cdot\eta\left(s_{fw};b_w;f_{cm};\bar{L}_{Rfi}\right) \tag{23}$$

3.3.5 Shear strength contribution provided by a system of ETS steel bars

Once the equivalent value of average resisting bond length is calculated, the effective capacity of the ETS bar $V_{fi,eff}^{\max}$ can be evaluated, as the minimum between the resisting bond force, V_f^{bd}, and the yield force, V_f^{y}, of the ETS bar:

$$V_{fi,eff}^{\max}=\min\left(V_f^{bd};V_f^{y}\right) \tag{24}$$

where V_f^{y} is obtained from Eq. (9) and V_f^{bd} is determined according to the simplified the bond-based constitutive law (Appendix A):

$$V_f^{bd}\left(\bar{L}_{Rfi}^{eq}\right)=L_p\cdot\frac{1}{J_1}\cdot\lambda\cdot\left\{\delta_1\cdot\sin\left(\lambda\cdot\bar{L}_{Rfi}^{eq}\right)\right\} \tag{25}$$

Finally, the ETS shear strength contribution can be obtained as follows:

$$V_f^{II}=n\cdot N_{f,\mathrm{int}}^{l}\cdot V_{fi,eff}^{\max}\cdot\sin\beta_f \tag{26}$$

where n is the number of installed bars in the cross section.

4 Models appraisal

The proposed formulations were used to calculate the ETS contribution of the tested beams presented in section 2, as well as the RC beams tested by Valerio et al [1] and Barros and Dalfré [3]. Those two experimental programs were characterized by

different test set-up, amount of longitudinal and transversal reinforcement, percentage and inclination of the strengthening system, and concrete compressive strength. Only the specimens failed in shear were considered in this study, and beams with unexpected behavior (for example 4S-S300-90) were also not considered. The beams tested by Valerio et al. were characterized by a cross section 350x450mm^2, a steel flexural reinforcement ratio of ρ_{sl} =0.93% and a L_1/d ratio of 4. The experimental program carried out by Barros and Dalfré [3] was characterized by two series of beams: A Series (150x300mm^2) and B series (300x300mm^2), with a ρ_{sl} of 2.5% and 1.88%, respectively, and a constant L_1/d ratio of 3.44. The main data of these experimental programs are reported in Table 3.

4.1 Validation of the Experimental based model

The values of ε_{fe} calculated with Eq. (7) are plotted in Fig. 9 as a function of $\left(E_{fw}\rho_{fw}+E_{sw}\rho_{sw}\right)/\left(f_{cm}{}^{2/3}\right)$, and for the two considered inclinations of the ETS bars (β_f). The term $\left(E_{fw}\rho_{fw}+E_{sw}\rho_{sw}\right)$ expresses the stiffness of the internal shear reinforcement and the shear strengthening; $\left(f_{cm}^{2/3}\right)$ reflects the influence of the concrete tensile strength. The equation for the evaluation of ε_{fe} that best fits the experimental results is the following one:

$$\varepsilon_{fe}^{I} = -0.099\cdot\left\{\left(E_{fw}\rho_{fw}+E_{sw}\rho_{sw}\right)/\left(f_{cm}{}^{2/3}\right)\right\} - 0.003\cdot\beta_f + 0.456 \qquad (27)$$

The values of ε_{fe} (Eq. 7) and the analytical values of the steel effective strain ε_{fe}^{I} (Eq. 27) are calculated for all of the beams presented in Table 1 and Table 3; the obtained results are collected in Table 4. Fig 9 shows the comparison between the experimental effective strain, ε_{fe}, and the analytical effective strain, ε_{fe}^{I}. In Fig. 9 the dotted line indicates the yield strain of the ETS bars, that limits the steel stress. In general the ε_{fe} for inclined ETS bars exceeded the yield strain, having reached the value of 0.40%, while vertical ETS bars presented average effective strain lower than the yield strain. Eq. (27) provides a different ε_{fe}^{I} - $\left(E_{fw}\rho_{fw}+E_{sw}\rho_{sw}\right)/\left(f_{cm}{}^{2/3}\right)$ relationship for different β_f values, with larger ε_{fe}^{I} values for the β_f =45°, as was observed experimentally.

The higher shear strengthening effectiveness of inclined ETS is captured by the model as is clearly shown in Fig. 9. The values of ε_{fe}^{I} exhibited a tendency to slightly decrease with the increase of $\left(E_{fw}\rho_{fw}+E_{sw}\rho_{sw}\right)/\left(f_{cm}{}^{2/3}\right)$. However, the

decay of the effective strain with the increase of $\left(E_{fw}\rho_{fw}+E_{sw}\rho_{sw}\right)\Big/\left(f_{cm}{}^{2/3}\right)$ is much smaller than in FRP-based techniques [19,22]. The available data is relatively small for this type of approach, and the dispersion of results is high; a larger number of specimens is required for a better model assessment.

The analytical values, V_f^I, are evaluated according to Eq. (5), where the effective stress of the ETS bars is given by the following Eq. (28):

$$f_{fe}=\begin{cases}\varepsilon_{fe}^I\cdot E_f & if \quad \varepsilon_f^I\le\varepsilon_{sy}\\ f_y & if \quad \varepsilon_f^I>\varepsilon_{sy}\end{cases} \tag{28}$$

The analytical values, V_f^I, and the corresponding experimental values, $V_f^{\exp}$, are included in Table 4. The graphical comparison between V_f^I and $V_f^{\exp}$ is presented in Fig. 10. Two lines limiting the deviation of the predicted values from the experimental ones at $\pm$ 30% are also depicted in Fig 10. It is easy to recognize that almost all of the results fall within these bounds. By determining The value of the ratio $k^I=V_f^{\exp}\big/V_f^I$ for all the considered beams, also included in Table 4, an average value of 1.08 and a standard deviation of 0.28 were obtained.

The design values of the ETS shear strengthening contribution V_{fd}^I are reported in Table 4. These values are calculated introducing the partial safety factor γ_f to the ε_{fe}^I, resulting a design effective strain $\varepsilon_{fd}=\varepsilon_{fe}^I/\gamma_f$, whose values are also indicated in Table 4. A value $\gamma_f=1.3$ is adopted in order to obtain design values for the ETS shear strengthening contribution, V_{fd}^I, lower than the experimental ones $\left(V_f^{\exp}\right)$ for the 90% of the analyzed beams, assuring a proper design safety format for this model. The V_{fd}^I vs $V_f^{\exp}$ is also represented in Fig. 10, and the values $V_f^{\exp}\big/V_{fd}^I$ of are presented in Table 4, resulting an average value of 1.30 for the ratio $V_f^{\exp}\big/V_{fd}^I$, which seems acceptable for a technique where the strengthening reinforcements are protected from the aggressiveness of environment agents and vandalism acts .

4.2 Validation of the Mechanical based model

According to Bianco et al. [42], the angle α defining the opening of the concrete fractured cone is set equal to 28.5°, but an interval between 20° and 30° was found in the literature [49,50]. The simplified bond model is characterized by τ_0 =16 MPa

and δ_1 =6 mm. The value of bond strength τ_0 and free-end slip δ_1 are selected taking into account the bond constitutive model for cast-in ribbed bars presented in the Model Code 2010 [51], and the experimental tests of embedded bars glued to concrete with epoxy adhesive available in literature [1,34,52–54] and reported in Breveglieri [55].

Regarding the present model, a sensitivity analysis to study the influence of each input parameter has been carried out by Bianco et al. [24], demonstrating that using the proposed simplified bond model the results are not significantly affected by changing the values of τ_0 and δ_1, but they are significantly affected by the values attributed to θ and α.

The predicted values V_f^{II} obtained by the formulation proposed in section 3.3 are presented in Table 5. V_f^{II} is the minimum between $V_f^{II,bd}$, and $V_f^{II,y}$, the strengthening contribution of the ETS system corresponding to the debonding and steel yielding of the ETS bars, respectively. The design values V_{fd}^{II} are also presented in Table 5, where a γ_f partial safety factor equal to 1.3 is assumed, in order to obtain design values lower than the experimental values for the 90% of the analyzed beams.

The analytical predictions, V_f^{II}, their corresponding design values, V_{fd}^{II}, and the experimental results, $V_f^{\exp}$, are compared in Fig. 11. The two lines limiting the deviation of the predicted values from the experimental values to $\pm$30% are also represented in Fig 11. Almost all of the results fall within these bounds. The values of the ratio $k^{II} = V_f^{\exp} / V_f^{II}$, included in Table 5, have an average value of 1.21 and a standard deviation of 0.42, while when using the design values V_{fd}^{II}, an average value of 1.57 was obtained for the k^{II} ratio (values within round brackets in Table 5).

In the cases where more than one ETS bar is installed in a cross section, a detrimental interaction effect on the strengthening capacity of each bar should be considered. For the analyzed beams the present model can simulate this interaction by limiting the width of the concrete prims to $b_w/2$; this assumption can be generalized by limiting the width of the concrete prism to the space between the bars in the same section of the beam, and checking for geometric compatibility**.**

Since this mechanical model neglects the influence of the existing steel stirrups on the ETS strengthening contribution, for each ETS strengthening solution there is a single V_f^{II}, independent from the percentage of existing stirrups, which is not supported by the experimental results (Fig. 5). A reduction factor, function of the internal transverse steel reinforcement, could be introduced, as proposed for EBR and NSM strengthening [30,40,56–58].

Like the experimental-based model, the mechanical-based model is able to differentiate between yield and debonding failure, as proved by the results reported in Table 5.

5. Conclusion

This paper presents the results of an experimental program on RC beams strengthened in shear using the ETS technique. The effectiveness of this technique was evaluated by studying the influence of three shear reinforcement ratio of existing steel stirrups (ρ_{sw} = 0%,0.10%,0.17%), spacing (300mm and 180mm) and inclination (90° and 45°) of steel ETS bars. The data obtained in the experimental program carried out, together with the experimental results available in literature dealing with the ETS technique were used to assess the predictive performance of two analytical approaches, denominated as *experimental-based* and *mechanical based* that were herein proposed for the estimation of the shear strengthening contribution assured by steel ETS bars.

The tested strengthened ETS beams exhibited a significant increase of load carrying capacity and deflection capacity for both vertical and inclined bars. However, the configuration with inclined bars has assured a much higher effectiveness, which is justified by the fact that for this latter configuration a higher available bond length was assured. Inclined bars were able to mobilize integrally the strength capacity of the ETS shear reinforcement, while in vertical ETS bars the resisting bond length of the bars crossed by the critical shear crack may have been not enough to mobilize its yield strain. As expected, the effectiveness of the ETS technique has decreased with the percentage of existing steel stirrups, especially for vertical ETS bars. The obtained results demonstrate that the ETS shear strengthening technique is an effective and competitive solution.

In terms of analytical models, the so called "experimental-based approach" is based on the concept of effective strain $\left(\varepsilon_{fe}^{I}\right)$, and an equation was proposed to obtain ε_{fe}^{I}. This equation is dependent of the ETS orientation β_f and of the parameter $\left(E_{fw}\rho_{fw}+E_{sw}\rho_{sw}\right)\Big/\left(f_{cm}^{2/3}\right)$ that includes the percentage of ETS $\left(\rho_{fw}\right)$, the percentage of steel stirrups $\left(\rho_{sw}\right)$ and the concrete compressive strength $\left(f_{cm}\right)$. The analytical $\left(V_f^I\right)$ and the experimental $\left(V_f^{\exp}\right)$ results of the ETS shear contribution were compared considering the ratio k $\left(k^I = V_f^{\exp}\big/V_f^I\right)$, whose average value was 1.08. This formulation provided satisfactory results, and evidenced the clearly different behavior between vertical and inclined strengthening, by detecting the steel yielding only in 45° installed bars.

The so-called "mechanical-based approach" is derived from a previous analytical model developed for NSM shear strengthened beams. This model is conceptually more reliable since it considers a bond constitutive law to evaluate the contribution of a single ETS bar, as well as the concrete fracture by reducing the available resisting bond length with the progress of the concrete fracture. The formulation provided satisfactory results, and the analytical $\left(V_f^{II}\right)$ and the experimental $\left(V_f^{\exp}\right)$ results of the ETS shear contribution were compared considering the ratio k ($k^{II} = V_f^{\exp} \big/ V_f^{II}$), whose average value was 1.21.

The two conceptually different approaches have predicted values with similar level of accuracy, however the experimental-based approach has provided a dispersion of results lower than the mechanical-based model. Nevertheless, in terms of structural safety, by adopting for both approaches a partial safety factor of γ_f =1.3, the shear strengthening contribution of 90% of the analyzed beams is less than the one recorded experimentally.

Acknowledgements

The authors wish to acknowledge the support provided by the CutInov project QREN n. 38780 supported by ADI, and by the Engineering Department of the University of Ferrara.

Appendix

Bond-based constitutive law

For a generic, transfer length $L_{Rfi} \le L_{Rfe}$, the relevant bond-based constitutive law $V_{fi}^{bd}\left(L_{Rfi}, \delta_{Li}\right)$ is considered as in Bianco et al. [36] neglecting the post-peak branch, and it is valid for values of $V_{fi}^{bd} \le V_{f1}^{bd}$:

$$V_{fi}^{bd}\left(L_{Rfi}, \delta_{Li}\right) = L_p \cdot J_3 \cdot \lambda \cdot \left\{C_1 \cdot \left[\cos\left(\lambda \cdot L_{Rfi}\left(\delta_{Li}\right)\right) - 1\right] - C_2 \cdot \sin\left(\lambda \cdot L_{Rfi}\left(\delta_{Li}\right)\right)\right\} \quad \text{(A.1)}$$

With the bond transfers length function of the δ_{Li} as follows:

$$L_{Rfi}\left(\delta_{Li}\right) = \frac{1}{\lambda} \cdot arc\cos\left(1 - \frac{\lambda^2}{\tau_0 \cdot J_1} \cdot \delta_{Li}\right) \quad \text{(A.2)}$$

For the resisting bond length $\left(L_{Rfi} \le L_{Rfe}\right)$, the imposed end slip defining the extremities of the bond based law is defined by the equation:

$$\delta_{Li}\left(L_{Rfi}\right) = C_1 \cdot \sin\left(\lambda \cdot L_{Rfi}\right) + C_2 \cdot \cos\left(\lambda \cdot L_{Rfi}\right) + \left(\tau_0 \cdot J_1 / \lambda^2\right) \tag{A.3}$$

With bond modelling constants [25,42] for a ETS bar embedded in a concrete prism:

$$\frac{1}{\lambda^2} = \frac{\delta_1}{\tau_0 \cdot J_1};\ J_1 = \frac{L_p}{A_{fw}}\left[\frac{1}{E_{fw}} + \frac{A_{fw}}{A_c \cdot E_c}\right];\ J_2 = \frac{E_{fw} \cdot E_c \cdot A_c}{E_c \cdot A_c + E_{fw} \cdot A_{fw}}\ \ J_3 = \frac{E_{fw} \cdot A_{fw} \cdot E_c \cdot A_c}{L_p\left(A_c \cdot E_c + A_{fw} \cdot E_{fw}\right)};$$

$$C_1 = \delta_1 - \frac{\tau_0 \cdot J_1}{\lambda^2};\ \ C_2 = -\frac{\tau_0 \cdot J_1}{\lambda^2};\ C_3 = \frac{V_f^y \cdot J_1}{L_p \cdot \lambda} \tag{A.4}$$

Calculation of f_{ctm}^*

The simplified model described in considered and equivalent bond length to account the concrete fracture by means of η and f_{ctm}^*. The concrete mean tensile strength, f_{ctm}^* is the value, beyond which concrete is not fractured and the average available resisting bond length is not reduced $(\eta = 1)$. The value of f_{ctm}^* can be determinate by imposing the equality $V_{fi}^{bd} = V_{fi}^{cf}$ between the concrete fracture capacity V_{fi}^{cf} and the corresponding maximum value of the bond transferred force V_{fi}^{bd}. This latter will be attained for a transfer length that is equal to L_{Rfi} (Eq. 22). In general it can be written:

$$V_{fi}^{cf}\left(L_{Rfi}\right) = V_{fi}^{bd}\left(L_{Rfi}\right) \tag{A.5}$$

The concrete fracture capacity can be calculated by spreading f_{ctm} thorough the semi-conical surface with o the cone, orthogonally to it in each point and integrating, as demonstrated by Bianco [42] the calculation can be reduced to the evaluation of the area of the ellipse intersection of the cone with the crack plane. Since in the present work the interaction between the ETS bars along the axis is not evaluated the cone opening was limited by the spacing of the ETS bars along the longitudinal axis $\left(s_{fw} \cdot \sin\beta_f\right)/\left(\sin\left(\theta + \beta_f\right)\right)$ and by $b_w/4$ in the orthogonal direction.

$$V_{fi}^{cf} = f_{ctm} \cdot \pi \cdot \min\left\{L_{Rfi} \cdot \tan\alpha; \frac{b_w}{4}\right\} \cdot \frac{\sin\left(\theta+\beta_f\right)}{2} \cdot \left(\min\left\{ \frac{s_{fw} \cdot \sin\beta_f}{2 \cdot \sin\left(\theta+\beta_f\right)}; \frac{L_{Rfi} \cdot \sin\alpha}{\sin\left(\beta_f+\theta+\alpha\right)} \right\} + \min\left\{ \frac{s_{fw} \cdot \sin\beta_f}{2 \cdot \sin\left(\theta+\beta_f\right)}; \frac{L_{Rfi} \cdot \sin\alpha}{\sin\left(\beta_f+\theta-\alpha\right)} \right\} \right) \quad \text{(A.6)}$$

The bond transferred force is given by Eq. (A.1), adopting simplification in Eq. (A.4). Since $J_3 = 1/J_1$, J_3 will be eliminated and substituted, whenever it appears, by $1/J_1$;since $\frac{1}{\lambda^2} = \frac{\delta_1}{\tau_0 \cdot J_1}$, C_1 vanishes and C_2 can be written as $C_2 = -\delta_1$, it results:

$$V_{fi}^{bd}\left(L_{Rfi}\right) = L_p \cdot \frac{1}{J_1} \cdot \lambda \cdot \delta_1 \cdot \sin\left(\lambda \cdot L_{Rfi}\right) \quad \text{(A.7)}$$

Substituting this latter in Eq. A.5 the f_{ctm}^{*} in Eq. (21) is obtained.

References

[1] Valerio P, Ibell TJ, Darby AP. Deep embedment of FRP for concrete shear strengthening. Proc ICE - Struct Build 2009;162(5):311–21. http://dx.doi.org /10.1680/stbu.2009.162.5.311

[2] Chaallal O, Mofidi A, Benmokrane B, Neale K. Embedded Through-Section FRP Rod Method for Shear Strengthening of RC Beams: Performance and Comparison with Existing Techniques. J Compos Constr 2011;15(3):732–42. http://dx.doi.org/10.1061/(ASCE)CC.1943-5614.0000174.

[3] Barros JAO, Dalfré GM. Assessment of the Effectiveness of the Embedded Through-Section Technique for the Shear Strengthening of Reinforced Concrete Beams. Strain 2012;49(1):75–93. http://dx.doi.org/10.1111/str.12016

[4] Breveglieri M, Aprile A, Barros JAO. Shear strengthening of reinforced concrete beams strengthened using embedded through section steel bars. Eng Struct 2014;81:76–87. http://dx.doi.org/10.1016/j.engstruct.2014.09.026

[5] Breveglieri M, Aprile A, Barros JAO. Embedded Through-Section shear strengthening technique using steel and CFRP bars In RC beams of different percentage of existing stirrups. Compos Struct 2015;125:101–13. http://dx.doi.org/10.1016/j.compstruct.2015.02.025

[6] Pelà L, Aprile A, Benedetti A. Experimental study of retrofit solutions for damaged concrete bridge slabs. Compos Part B Eng 2012;43(5):2471–9. http://dx.doi.org/10.1016/j.compositesb.2011.08.038

[7] Bianco V, Barros JAO, Monti G. Bond model of NSM CFRP in the context of the shear strengthening of RC beams. ASCE J Struct Eng 2009;135(6):619–31. http://dx.doi.org/10.1061/(ASCE)0733-9445(2009)135:6(619)

[8] Mohamed Ali MS, Oehlers DJ, Griffith MC, Seracino R. Interfacial stress transfer of near surface-mounted FRP-to-concrete joints. Eng Struct 2008;30(7):1861–8. http://dx.doi.org/10.1016/j.engstruct.2007.12.006

[9] Yuan H, Teng JG, Seracino R, Wu ZS, Yao J. Full-range behavior of FRP-to-concrete bonded joints. Eng Struct 2004;26(5):553–65. http://dx.doi.org/10.1016/j.engstruct.2003.11.006

[10] Oehlers DJ, Haskett M, Wu C, Seracino R. Embedding NSM FRP plates for Improved IC debonding resistance. J Compos Constr 2008;12(6):635–42. http://dx.doi.org/10.1061/(ASCE)1090-0268(2008)12:6(635)

[11] Perrone M, Barros JAO, Aprile A. CFRP-Based Strengthening Technique to Increase the Flexural and Energy Dissipation Capacities of RC Columns. J Compos Constr 2009;13(5):372–83. http://dx.doi.org 10.1061/(ASCE)CC.1943-5614.0000031

[12] Lima JLT, Barros JAO. Reliability analysis of shear strengthening externally bonded FRP models. Proc ICE - Struct Build 2011;164(1):43–56. http://dx.doi.org/10.1680/stbu.9.00042

[13] Bousselham A, Chaallal O. Mechanisms of Shear Resistance of Concrete Beams Strengthened in Shear with Externally Bonded FRP. J Compos Constr 2008;12(5):499–512. http://dx.doi.org/10.1061/(ASCE)1090-0268(2008)12:5(499)

[14] Belarbi A, Kuchma DA, Okeil AM, Bae S-W. Design Equations for Shear Capacity of Concrete Girders Strengthened in Shear with Externally Bonded FRP Sheets. In: Proc: Asia-Pacific Conference on FRP in Structures (APFIS), Hokkaido University Japan 2-4 February 2012, p. 8.

[15] Fib – Bulletin 14. Externally bonded FRP reinforcement for RC structures. Technical report by Task Group 9.3 FRP (Fiber Reinforced Polymer) reinforcement for concrete structures, Féderation Internationale du Béton – fib; July 2001.

[16] CAN/CSA-S806-02. Design and construction of building components with fibrereinforced polymer. Canadian Standards Association, Rexdale, Canada; 2002.

[17] American Concrete Institute. Guide for the design and con- struction of externally bonded FRP systems for strengthening concrete structures. ACI440.2R. Farmington Hills, MI: American Concrete Institute, Detroit; 2008.

[18] National Research Council 2004. Guide for design and construction of externally bonded FRP systems for strengthening existing structures CNR-DT200 2012.

[19] Triantafillou T. Shear Strengthening of Reinforced Concrete Beams Using Epoxy-Bonded FRP Composites. ACI Struct J 1998;95(2):107–15. http://dx.doi.org/10.14359/531

[20] Triantafillou T., Antonopoulos CP. Design of concrete flexural members strengthened in shear with FRP. J Compos Constr 2000;4(4):198–205. http://dx.doi.org/10.1061/(ASCE)1090-0268(2000)4:4(198)

[21] Chaallal O, Nollet M-J, Perraton D. Strengthening of reinforced concrete beams with externally bonded fiber-reinforced-plastic plates: design guidelines for shear and flexure. Can J Civ Eng 1998;25(4):692–704. http://dx.doi.org/10.1139/l98-008

[22] Dias SJE, Barros JAO. Shear strengthening of RC beams with NSM CFRP laminates: Experimental research and analytical formulation. Compos Struct 2013;99:477–90. http://dx.doi.org/10.1016/j.compstruct.2012.09.026

[23] Khalifa A, Gold WJ, Nanni A, M.I. AA. Contribution of Externally Bonded FRP to Shear Capacity of RC Flexural Members. J Compos Constr 1998;2(4):195–202. http://dx.doi.org/10.1061/(ASCE)1090-0268(1998)2:4(195)

[24] Bianco V, Monti G, Barros JAO. Design formula to evaluate the NSM FRP strips shear strength contribution to a RC beam. Compos Part B Eng 2014;56:960–71. http://dx.doi.org/10.1016/j.compositesb.2013.09.001

[25] Bianco V, Barros JAO, Monti G. Three dimensional mechanical model for simulating the NSM FRP strips shear strength contribution to RC beams. Eng Struct 2009;31(4):815–26. http://dx.doi.org/10.1016/j.engstruct.2008.12.017

[26] Bianco V, Barros JAO, Monti G. New approach for modeling the contribution of NSM FRP strips for shear strengthening of RC beams. J Compos Constr 2010;14(1):36–48. http://dx.doi.org/10.1061/(ASCE)CC.1943-5614.0000048

[27] Dias SJE, Barros JAO. Performance of reinforced concrete T beams strengthened in shear with NSM CFRP laminates. Eng Struct 2010;32(2):373–84. http://dx.doi.org/10.1016/j.engstruct.2009.10.001

[28] Carolin A, Täljsten B. Theoretical Study of Strengthening for Increased Shear Bearing Capacity. J Compos Constr 2005;9(6):497–506. http://dx.doi.org/10.1061/(ASCE)1090-0268(2005)9:6(497)

[29] Malek AM, Saasatmanesh H. Ultimate Shear Capacity of Reinforced Concrete Beams Strengthened with Web-Bonded Fiber-Reinforced Plastic Plates. ACI Struct J 1998;95(4):391–9. http://dx.doi.org/10.14359/555

[30] Chaallal O, Mofidi A. Shear Strengthening of RC Beams with Externally Bonded FRP Composites: Effect of Strip-Width-to-Strip-Spacing Ratio. J Compos Constr 2011;15(5):732–42. http://dx.doi.org/10.1061/(ASCE)CC.1943-5614.0000219

[31] Täljsten B. Strengthening concrete beams for shear with CFRP sheets. Constr Build Mater 2003;17(1):15–26. http://dx.doi.org/10.1016/S0950-0618(02)00088-0

[32] Chen JF, Teng JG. Shear capacity of FRP-strengthened RC beams: FRP debonding. Constr Build Mater 2003;17(1):27–41. http://dx.doi.org/10.1016/S0950-0618(02)00091-0

[33] Aprile A, Benedetti A. Coupled flexural-shear design of R/C beams strengthened with FRP. Compos Part B Eng 2004;35(1):1–25. http://dx.doi.org/10.1016/j.compositesb.2003.09.001

[34] Dalfré GM, Barros JAO, Machado D. Steel bar – concrete bond behavior in the context of the ETS shear strengthening technique for RC beams. In: Proc: 53° Brazilan Conference on Concret – IBRACON, Florianopolis, November 2011. p. 15.

[35] Mofidi A, Chaallal O. Shear Strengthening of RC Beams with EB FRP: Influencing Factors and Conceptual Debonding Model. J Compos Constr 2011;15(1):62–74. http://dx.doi.org/10.1061/(ASCE)CC.1943-5614.0000153

[36] Bianco V, Monti G, Barros JA. Theoretical Model and Computational Procedure to Evaluate the NSM FRP Strips Shear Strength Contribution to a RC Beam. J Struct Eng 2011;137(11):1359–72. http://dx.doi.org/10.1061/(ASCE)ST.1943-541X.0000370.

[37] Rizzo A, De Lorenzis L. Behavior and capacity of RC beams strengthened in shear with NSM FRP reinforcement. Constr Build Mater 2009(4);23:1555–67. http://dx.doi.org/10.1016/j.conbuildmat.2007.08.014

[38] Dias SJE, Barros JAO. Shear strengthening of RC T-section beams with low strength concrete using NSM CFRP laminates. Cem Concr Compos 2011;33(2):334–45. http://dx.doi.org/10.1016/j.cemconcomp.2010.10.002

[39] Bousselham A, Chaallal O. Effect of transverse steel and shear span on the performance of RC beams strengthened in shear with CFRP. Compos Part B Eng 2006;37(1):37–46. http://dx.doi.org/10.1016/j.compositesb.2005.05.012

[40] Pellegrino M, Modena C. Fiber-Reinforced Polymer Shear Strengthening of Reinforced Concrete Beams: Experimental Study and Analytical Modeling. ACI Struct J 2006;103(5):720–8. http://dx.doi.org/10.1016/10.1061/(ASCE)1090-0268(2002)6:2(104)

[41] Grande E, Imbimbo M, Rasuolo A. Effect of transverse steel on the response of RC beams strengthened in shear by FRP: Experimental study. J Compos Constr 2009;13(9):405–14. http://dx.doi.org/10.1061/(ASCE)1090-0268(2009)13:5(405)

[42] Bianco V. Shear Strengthening of RC beams by means of NSM CFRP strips: experimental evidence and analytical modeling, PhD Thesis, Department of Structural Engineering and Geotechnics, Sapienza University of Rome, Rome, Italy, December 2008.

[43] Paulay T. Coupling Beams of Reinforced Concrete Shear Walls. J Struct Div 1971;97(3):843–62.

[44] Bousselham A, Chaallal O. Shear Strengthening Reinforced Concrete Beams with Fiber-Reinforced Polymer: Assessment of Influencing Parameters and Required Research. ACI Struct J 2004;101(2):219–27. http://dx.doi.org/10.14359/13019

[45] Cao SY, Chen JF, Teng JG, Hao Z, Chen J. Debonding in RC Beams Shear Strengthened with Complete FRP Wraps. J Compos Constr 2005;9(5):417–28. http://dx.doi.org/10.1061/(ASCE)1090-0268(2005)9:5(417))

[46] Mohamed Ali MS, Oehlers DJ, Seracino R. Vertical shear interaction model between external FRP transverse plates and internal steel stirrups. Eng Struct 2006;28(3):381–9. http://dx.doi.org/10.1016/j.engstruct.2005.08.010

[47] Monti G, Liotta M. Tests and design equations for FRP-strengthening in shear. Constr Build Mater 2007;21(4):799–809. http://dx.doi.org/10.1016/j.conbuildmat.2006.06.023

[48] CEB-FIP Model Code 90, Bulletin d'Information N° 213/214.Th. Telford, London, 1993; ISBN 0-7277-1696-4: 460 pages.

[49] Teng JG, De Lorenzis L, Wang B, Li R, Wong TN, Lam L. Debonding Failures of RC Beams Strengthened with Near Surface Mounted CFRP Strips. J Compos Constr 2006;10(2):92–105. http://dx.doi.org/10.1061/(ASCE)1090-0268(2006)10:2(92)

[50] Bianco V, Barros JAO, Monti G. Shear Strengthening of RC beams by means of NSM laminates: experimental evidence and predictive models Report 06-DEC/E-18. Universidade do Minho, Guimaraes: 2006.

[51] fib Model Code for Concrete Structures 2010. Ernst & Sohn; 2013, ISBN: 978-3-433-03061-5: 434 pages

[52] Mahrenholtz C. Seismic bond model for concrete reinforcement and the application to column-to-foundation connections. Phd Thesis, Institut für Werkstoffe im Bauwesen der Universität Stuttgart, University in Stuttgart, Germany, 2012.

[53] Owa S, Yamamoto Y, Kondo T, Fogstad C. Study on Strength and Ductility of Post-installed Adhesive Anchoring System –Comparison and analysis of experimental values, various values in ultimate strength and design strength. In. Proc: 15WCEE / 15th World Conf. Earthq. Eng. Lisbon, 2012.

[54] Godat A, L'Hady A, Chaallal O, Neale K. Bond Behavior of the ETS FRP Bar Shear-Strengthening Method. J Compos Constr 2012;16(5):529–30. http://dx.doi.org/10.1016/S0141-0296(01)00035-9

[55] Breveglieri M. Shear strengthening of RC beams using the Embedded Through-Section technique. Phd Thesis, Department of Engineering, Univesity of Ferrara, 2015.

[56] Chen GM, Teng JG, Chen JF. Shear Strength Model for FRP-Strengthened RC Beams with Adverse FRP-Steel Interaction. J Compos Constr 2013;17(1):50–66. http://dx.doi.org/10.1061/(ASCE)CC.1943-5614.0000313

[57] Chen GM, Teng JG, Chen JF, Rosenboom OA. Interaction between Steel Stirrups and Shear-Strengthening FRP Strips in RC Beams. J Compos Constr 2010;14(5):498–509. http://dx.doi.org/10.1061/(ASCE)CC.1943-5614.0000120

[58] Li A, Delmas Y. CRFP contribution to shear capacity of strengthened RC beams. Eng Struct 2001;23(10):1212–20. http://dx.doi.org/10.1016/S0141-0296(01)00035-9

Nomenclature

Latin Letters

A_c	area of the concrete prism cross section
A_{fw}	area of the strengthening
b_w	beam's width
CDC	critical diagonal crack (shear crack)
C_1, C_2, C_3	integration constants of the bond model
d	beam cross section effective depth
E_c	concrete Young's modulus
E_{fw}	strengthening Young's modulus
E_{sw}	internal reinforcement Young's modulus
f_{cm}	concrete average cylindrical compressive strength
f_{ctm}	concrete average tensile strength.
f_{ctm}^{*}	value of average concrete tensile strength for values larger than which concrete fracture does not occur
f_{fe}	effective stress in the ETS bar
f_y	steel yield stress
F	applied load
F_f	force resulting from the tensile stress in the ETS bars crossing the shear failure crack
$F_{\max}$	maximum load
$F_{\max,Ref}$	maximum load of the reference beam
h_w	beam cross section height
J_1, J_2, J_3	constants of the bond model
k	number expressing the safety factor of the model
L_1	strengthened beam's shear span length
L_d	crack length
L_f	strengthening ETS bar length
L_{fi}	available bond length for a single ith ETS bar
L_p	bar perimeter
L_{Rfe}	effective resisting bond length
L_{Rfi}	ith bar resisting bond length
$\bar{L}_{Rfi}$	average available bond length
$\bar{L}_{Rfi}^{eq}$	equivalent value of the average resisting bond length
n	number of installed bars in the considered cross section
n_f	number of ETS bars crossed by the shear failure crack
$N_{f,\text{int}}^{l}$	minimum integer number of bars that can cross the CDC
s_{fw}	ETS bars spacing
s_{sw}	stirrups spacing
V_f^{ana}	ETS analytical contribution
V_f^{I}	ETS contribution calculated with the experimental based-approach

V_f^{II}	ETS contribution calculated with the mechanical based-approach
V_{fd}^{I}	design value calculated using the experimental-based approach
V_{fd}^{II}	design value calculated using the mechanical-based approach
V_{f1}^{bd}	maximum value of the force transferable through bond by the given ETS bar
$V_{fi}^{bd}\left(L_{Rfi},\delta_{Li}\right)$	bond based constitutive law
V_f^{bd}	force transferred by bond capacity of a single ETS bars
$V_f^{II,bd}$	ETS contribution corresponding to the bond capacity
$V_f^{II,y}$	ETS contribution corresponding to the yield strength
V_{fi}^{cf}	concrete tensile fracture capacity
$V_f^{\exp}$	experimental value of the ETS contribution
$V_{fi,eff}^{\max}$	maximum effective capacity of the average-length bar along the CDC.
V_{Ref}	shear strength of a reference beam
V_f^{y}	yielding capacity of a single ETS bars
V_t	total shear strength
u_L	deflection
$u_{L\max}$	deflection at maximum load $F_{\max}$

Greek letters

α	angle between the axis and the generatrices of the concrete conical surface.
β_f	inclination of the strengthening with respect to the beam longitudinal axis.
γ_f	partial safety factor
δ_1	slip corresponding to the free-slipping in the local bond stress-slip relationship.
δ_{Li}	loaded end slip imposed.
ε_{fe}	effective strain
ε_{fe}^{I}	effective stain for the evaluation of the shear strengthening contribution of the ETS system
ε_{fd}	design effective strain
ε_{sy}	steel yield strain
η	reduction factor of the initial average available resisting bond length
θ	critical diagonal crack (CDC) inclination angle
λ	constant entering the governing differential equation for the bond elastic phase
ρ_{fw}	percentage of shear strengthening ratio
ρ_{sl}	percentage of steel longitudinal reinforcement.
ρ_{sw}	percentage of shear reinforcement ratio
τ_0	adhesive-cohesive initial bond strength of the local stress-slip relationship/Peak stress of the local bond stress-slip relationship
ϕ_f	ETS bar diameter
ϕ_s	stirrups diameter

TABLES CAPTIONS

Table 1 ETS shear strengthening configurations of the tested beams.

Table 2 Experimental results of 0S-Series, 2S-Series and 4S-Series.

Table 3 Experimental results of previous experimental tests on beams strengthened with ETS technique.

Table 4 Experiemental-based model assessment.

Table 5 Mechanical-based model assessemnt.

Table 1 ETS shear strengthening configurations of the tested beams.

Number of bars	Angle β_f [°]	ETS bar spacing [s_{fw}] (mm)	ETS Reinforcing ratio [ρ_{fw}][a] [%]	0S-Ref (ρ_{sw}=0.0%)[b]	$\rho_{sw}+\rho_{fw}$ [%]	2S-Ref (ρ_{sw}=0.10%)[b]	$\rho_{sw}+\rho_{fw}$ [%]	4S-Ref (ρ_{sw}=0.17%)[b]	$\rho_{sw}+\rho_{fw}$ [%]
3	90	300	0.15	0S-S300-90	0.15	2S-S300-90	0.25	4S-S300-90	0.32
3	45	300	0.21	0S-S300-45	0.21	2S-S300-45	0.31	4S-S300-45	0.38
5	90	180	0.24	0S-S180-90	0.24	2S-S180-90	0.35	4S-S180-90	0.42
5	45	180	0.34	0S-S180-45	0.34	2S-S180-45	0.45	4S-S180-45	0.52

[a] The ETS percentage was obtained from $\rho_{fw} = \left(A_{fw} / \left(b_w \cdot s_{fw} \cdot \sin \beta_f\right)\right) \times 100$ where A_{fw} area of the ETS bar cross section.

[b] The percentage of the vertical steel stirrups was obtained from $\rho_{sw} = (A_{sw} / (b_w \cdot s_{sw})) \times 100$ where A_{sw} is the cross sectional of the arms of a steel stirrup, and s_w is the spacing of the stirrups.

Table 2 Experimental results of 0S-Series, 2S-Series and 4S-Series.

	$F_{\max}$	$u_{L\max}$	$\Delta F/F_{\max,\mathrm{Re}f}$	V_t	$V_f^{\exp}$	CDC
	[kN]	[mm]	[%]	[kN]	[kN]	[°]
0S-Ref	156.1	4.66	--	93.6	--	39
0S-S300-90	217.8	4.37	39.5	130.7	37.0	42
0S-S300-45	348.6		123.4	209.2	115.5	47
0S-S180-90	256.8	4.31	64.6	154.1	60.5	44
0S-S180-45	368.8	6.56	136.3	221.3	127.7	43
2S-Ref	242.1	4.70	--	145.2	--	39
2S-S300-90	315.7	5.32	30.4	189.4	44.2	42
2S-S300-45	407.1	7.03	68.2	244.3	99.0	39
2S-S180-90	406.8	8.27	68.1	244.1	98.8	47
2S-S180-45	504.7	8.37	108.5	302.8	157.6	49
4S-Ref	353.8	7.35	--	212.3	--	40
4S-S300-90	370.9	7.43	4.8	222.6	10.3	46
4S-S300-45	552.4	12.03	56.1	331.5	119.2	54
4S-S180-90	413.2	6.32	16.8	247.9	35.6	54
4S-S180-45	566.4	11.01	60.1	339.8	127.6	40

Table 3 Experimental results of previous experimental tests on beams strengthened with ETS technique.

	β_f	Compressive strength	ρ_{sw}	ρ_{fw}	$\rho_{sw}+\rho_{fw}$	ϕ_s	s_{sw}	ϕ_f	s_{fw}
	[°]	[MPa]	[%]	[%]	[%]	[mm]	[mm]	[mm]	[mm]
Valerio et al. 2009 [1]									
SLB P4d-2S8@d	90°	[55-60][a]	0.00	0.09	0.09	--	--	2ϕ8	260
Dalfré and Barros 2012 [3]									
A.3 E300.90	90°	30.78[b]	0.00	0.17	0.17	--	--	ϕ10	300
A.4 E300.45	45°	28.81[b]	0.00	0.25	0.25	--	--	ϕ10	300
A.5 S300.90/E300.90	90°	30.78[b]	0.13	0.17	0.30	2ϕ6	300	ϕ10	300
B.3 E300.90	90°	30.78[b]	0.00	0.11	0.11	--	--	2ϕ8	300
B.4 E300.45	45°	28.81[b]	0.00	0.16	0.16	--	--	2ϕ8	300

[a] cubical compressive strength
[b] cylindrical compressive strength

Table 4 Experiemental-based model assessemnt.

Beam ID	V_f^{exp}	$\frac{\left(E_{fw}\rho_{fw}+E_{sw}\rho_{sw}\right)}{f_{cm}^{2/3}}$	ε_{fe}	V_f^I	$\varepsilon_{fd}=\frac{\varepsilon_{fe}}{\gamma_f}$	V_{fd}^I	k^I γ_f=1[a] (γ_f=1.3[b])
	[kN]	--	[%]	[kN]	[%]	[kN]	
Vertical							
0S-S300-90	37.017	0.030	0.18	39.60	0.14	30.46	0.93 (1.22)
0S-S180-90	60.453	0.051	0.17	65.30	0.13	50.23	0.93 (1.20)
2S-S300-90	44.199	0.052	0.21	39.14	0.13	30.11	1.13 (1.47)
2S-S180-90	98.847	0.072	0.28	64.54	0.13	49.65	1.53 (1.99)
4S-180-90	35.64	0.087	0.10	64.04	0.12	49.26	0.56 (0.72)
A-3 E300.90	31.15	0.036	0.19	30.37	0.14	23.36	1.03 (1.33)
A.5 S300.90/E300.90	40.3	0.063	0.25	29.94	0.13	23.03	1.35 (1.75)
B.3 E300.90	21.31	0.024	0.10	40.49	0.14	31.15	0.53 (0.68)
SLB P4d-2S8@d	53.2	0.030	0.20	51.63	0.14	39.72	1.03 (1.75)
Inclined							
0S-S300-45	115.53	0.043	0.39	81.5	0.25	72.9	1.42 (1.58)
0S-S180-45	127.66	0.071	0.26	135.8	0.24	120.5	0.94 (1.06)
2S-S300-45	99.036	0.065	0.33	81.5	0.25	72.4	1.22 (1.37)
2S-S180-45	157.6	0.093	0.32	135.8	0.24	119.6	1.16 (1.32)
4S-S300-45	119.18	0.079	0.40	81.5	0.24	72.1	1.46 (1.65)
4S-S180-45	127.58	0.108	0.26	135.8	0.23	119.1	0.94 (1.07)
A.4 S300.45	57.07	0.054	0.25	60.2	0.25	55.9	0.95 (1.02)
B.4 E300.45	98.52	0.036	0.33	80.3	0.25	74.5	1.23 (1.32)

[a]Average k^I (γ_f =1):1.08

[b]Average k^I(γ_f =1.3):1.30

Table 5 Mechanical-based model assessemnt.

Beam ID	$V_f^{\exp}$ [kN]	$V_f^{II,bd}$ [kN]	$V_f^{II,y}$ [kN]	Failure[a]	V_{fd}^{II} [kN]	k^{II} γ_f=1[b] (γ_f=1.3[c])
Vertical						
0S-S300-90	37.017	35.8	43.2	D	27.54	1.03 (1.34)
2S-S300-90	44.199					1.23 (1.60)
0S-S180-90	60.453	76.9	86.4	D	59.15	0.79 (1.02)
2S-S180-90	98.847					1.29 (1.67)
4S-S180-90	35.64					0.46 (0.60)
A-3 S300.90	31.15	24.9	42.5	D	19.18	1.25 (1.62)
A.5 S300.90/300.90	40.3					1.62 (2.1)
B.3 E300.90	21.31	46.5	56.9	D	35.73	0.46 (0.60)
SLB P4d-2S8@d	53.2	71.73	53.28	Y	40.99	1.00 (1.3)
Inclined						
0S-S300-45	115.53	94.6	61.1	Y	47.00	1.89 (2.46)
2S-S300-45	99.036					1.62 (2.11)
4S-S300-45	119.18					1.95 (2.54)
0S-S180-45	127.66	147.6	122.2	Y	94.00	1.04 (1.36)
2S-S180-45	157.6					1.29 (1.68)
4S-S180-45	127.58					1.04 (1.36)
A.4 E300.45	57.07	40.7	60.1	D	31.31	1.40 (1.82)
B.4 E300.45	98.52	89.99	80.5	Y	61.89	1.22 (1.59)

[a] Failure type basend on the analytical results: D, debonding, Y, yielding

[b]Average k^{II} ($\gamma_f = 1$):1.21

[c]Average k^{II}($\gamma_f = 1.3$):1.57

FIGURE CAPTIONS

Fig. 1. Tested beams: geometry, steel reinforcements applied in all beams. Beam 4S-S300-45 is presented: stirrups spaced at 180 mm and inclined ETS bars spaced at 300mm (all dimensions in mm).

Fig. 2 Tested strengthening arrangement: (a) 0S-S300-90, vertical ETS spaced at 300mm ; (b) 2S-S300-45, inclined ETS spaced at 300mm ,(c) 4S-S180-90, vertical ETS spaced at 180 mm ,(d) 4S-S180-45, inclined ETS spaced at 180 mm(dimensions in mm).

Fig. 3 Load deflection relationship for 2S-Series.

Fig. 4 Crack pattern beams: 0S-300-90, 0S-S180-90, 2S-300-45, 2S-S180-90, 2S-S180-45, 4S-S300-90, 4S-S180-90, 4S-S180-45.

Fig. 5. Influence of ρ_{fw} and ρ_{sw} on the $V_f^{\exp}$.

Fig. 6 Data for the analytical definition of the effective strain of the ETS system**.**

Fig. 7 Main mechanical features on the theoretical model and calculation procedure: (a) average-available-bond-length ETS bar and concrete cone of influence, (b) adopted bond stress-slip relationship, (c) ETS confined to the corresponding concrete prism of influence and conical surface fracture surface and area of the concrete cone at the CDC intersection, (d) Failure modes.

Fig. 8 Calculation procedure of the mechanical-based approach.

Fig. 9 Effective strain versus $\left(E_{fw}\rho_{fw}+E_{sw}\rho_{sw}\right)/\left(f_{cm}{}^{2/3}\right)$ from experimental data and obtained analitically.

Fig. 10 V_f^I and V_{fd}^I vs $V_f^{\exp}$ according to the experimental-based approach.

Fig. 11 V_f^{II} **and** V_{fd}^{II} vs $V_f^{\exp}$ according to the mechanical-based approach.

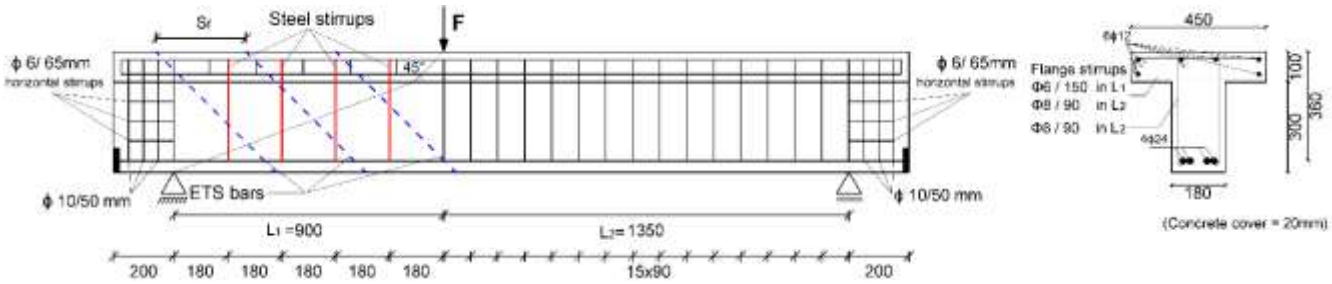

Fig. 1. Tested beams: geometry, steel reinforcements applied in all beams. Beam 4S-S300-45 is presented: stirrups spaced at 180 mm and inclined ETS bars spaced at 300mm (all dimensions in mm).

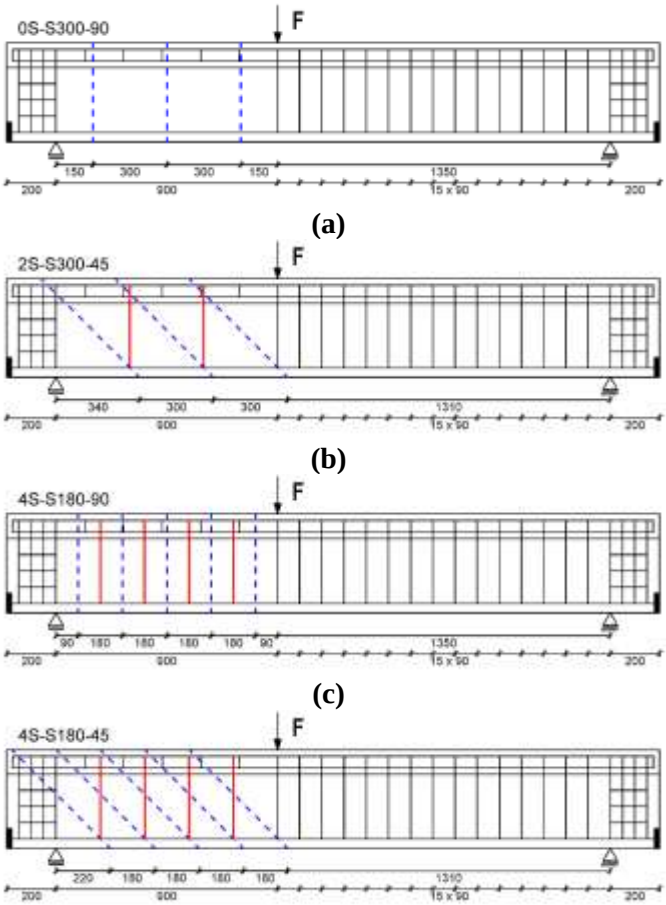

Fig. 2 Tested strengthening arrangement: (a) 0S-S300-90, vertical ETS spaced at 300 mm; (b) 2S-S300-45, inclined ETS spaced at 300 mm, (c) 4S-S180-90, vertical ETS spaced at 180 mm, (d) 4S-S180-45, inclined ETS spaced at 180 mm (dimensions in mm).

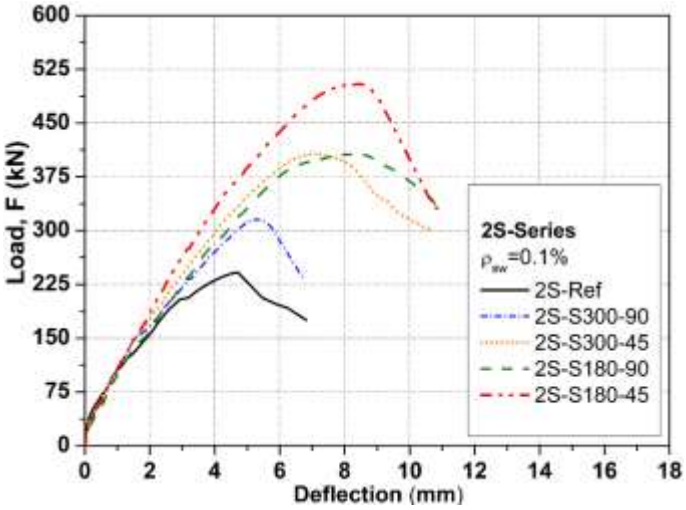

Fig. 3 Load deflection relationship for 2S-Series.

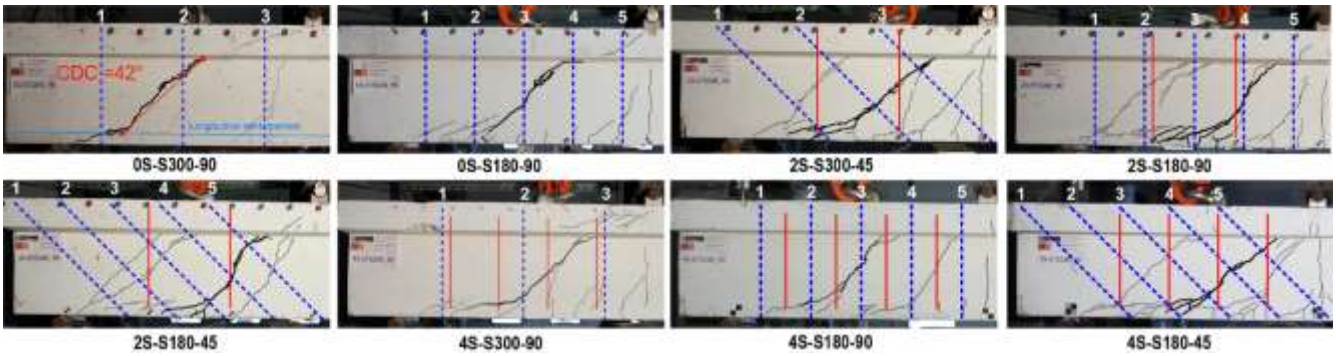

Fig. 4 Crack pattern beams: 0S-300-90, 0S-S180-90, 2S-300-45, 2S-S180-90, 2S-S180-45, 4S-S300-90, 4S-S180-90, 4S-S180-45.

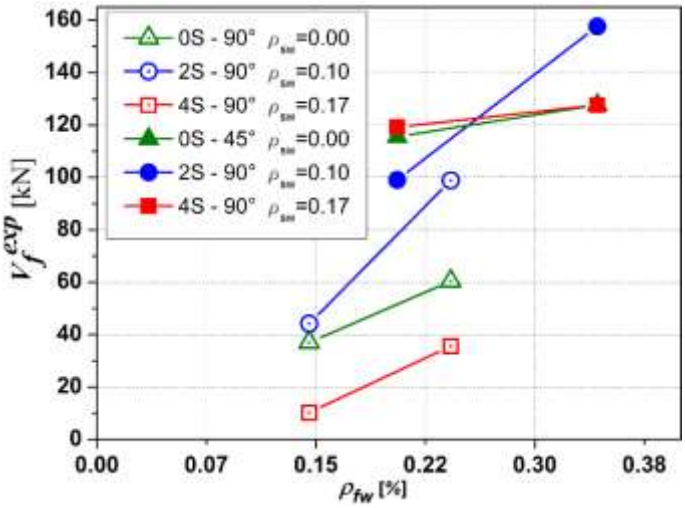

Fig. 5. Influence of ρ_{fw} and ρ_{sw} on the $V_f^{\exp}$.

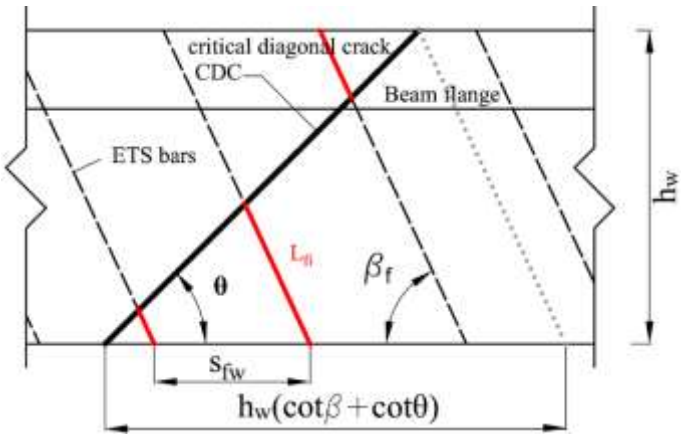

Fig. 6 Data for the analytical definition of the effective strain of the ETS system**.**

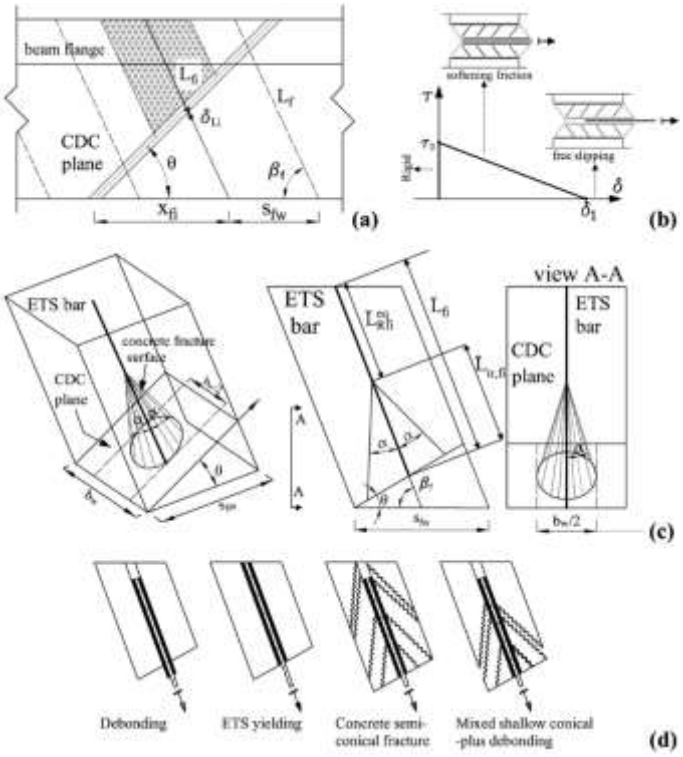

Fig. 7 Main mechanical features on the theoretical model and calculation procedure: (a) average-available-bond-length ETS bar and concrete cone of influence, (b) adopted bond stress-slip relationship, (c) ETS confined to the corresponding concrete prism of influence and conical surface fracture surface and area of the concrete cone at the CDC intersection, (d) Failure modes.

Input Parameters

$$h_w; b_w; \alpha;\ f_{cm}; s_{fw}; n; \beta_f;\ f_y; E_f; \phi_f; \tau_0; \delta_1; \theta$$

Evaluation of the average available resisting bond length and the minimum integer number of ETS bars effectively crossing the CDC

$$\overline{L}_{Rfi} = f\left(h_w; \theta; \beta_f; s_{fw}\right); N^{l}_{f,\text{int}}$$

Evaluation of constants

$$L_p; A_c; V_f^y; V_{f1}^{bd}; J_1; \lambda$$

Evaluation of the average available resisting bond length reduction factor, and the equivalent average resisting bond length

$$\eta = \left(s_{fw}; b_w;\ f_{ctm}; \overline{L}_{Rfi}\right); \overline{L}^{eq}_{Rfi}$$

Evaluation of the maximum effective capacity for one ETS bar

$$V^{\max}_{fi,eff} = \min\left(V_f^{bd}\ ; V_f^y\right)$$

Evaluation of the ETS bars contribution

$$V^{II}_{fd} = \frac{V^{II}_f}{\gamma_f} = \frac{1}{\gamma_f} \cdot \left(n \cdot N^{l}_{f,\text{int}} \cdot V^{\max}_{fi,eff} \cdot \sin\beta_f\right)$$

Fig. 8 Calculation procedure of the mechanical-based approach.

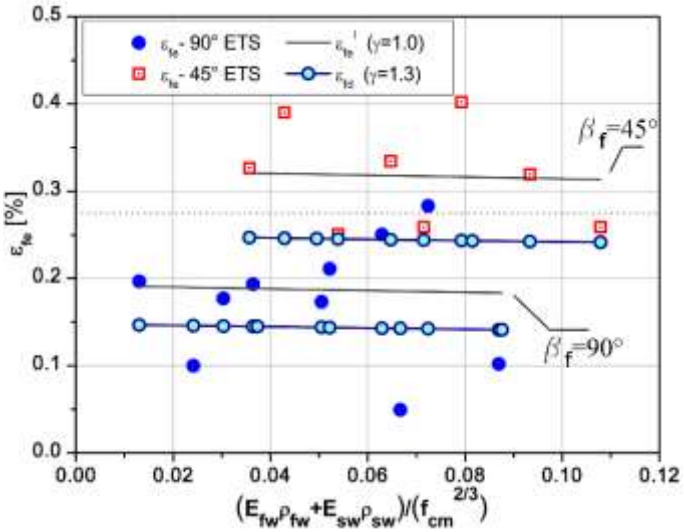

Fig. 9 Effective strain versus $\left(E_{fw}\rho_{fw}+E_{sw}\rho_{sw}\right)/\left(f_{cm}^{2/3}\right)$ from experimental data and obtained analitically.

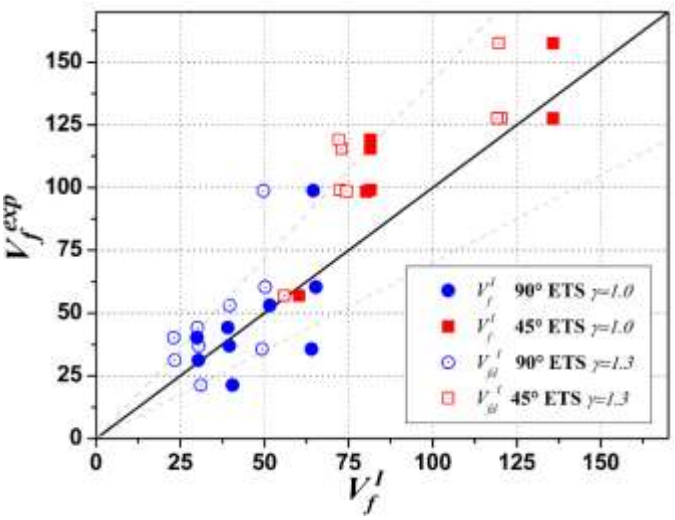

Fig. 10 V_f^I and V_{fd}^I vs $V_f^{\exp}$ according to the experimental-based approach**.**

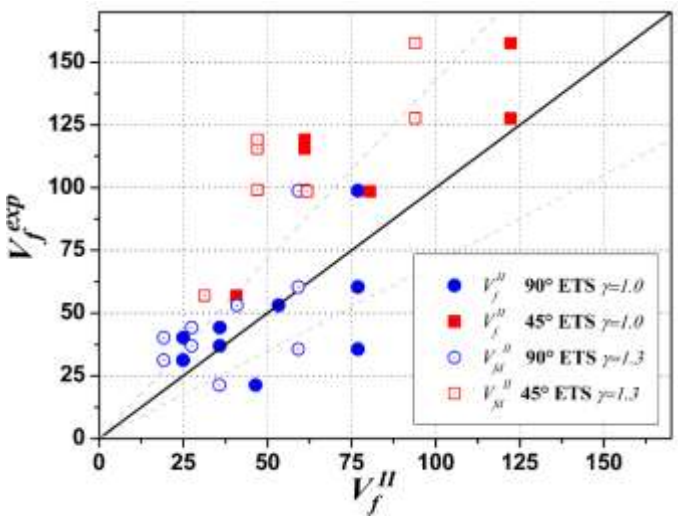

Fig. 11 V_f^{II} **and** V_{fd}^{II} vs $V_f^{\exp}$ according to the mechanical-based approach.